

# **Numerical Investigation of Electrohydrodynamic Effect on Lift and Drag Forces on an Airfoil in Low Reynolds Air Flow**

**M. Ashna\***

Department of Engineering, Sanandaj Branch,  
Islamic Azad University, Iran  
E-mail: m\_ashna@iausdj.ac.ir

\*Corresponding author

**Received: 2 April 2014, Revised: 4 November 2014, Accepted: 19 November 2014**

**Abstract:** Effect of forces due to electric field on two-dimensional low Reynolds air flow around an airfoil and variation of lift and drag coefficients are numerically investigated. The electric current and Gauss's equations are solved and the outcome is considered as a source term in momentum equations. The energy equation is not considered due to its weak effect on the phenomena. Finite volume method is used to solve both electrical and flow equations. Comparing results with an empirical work reveals that the numerical method gives tolerable results, where imposing high voltage electric field can alter the drag and lift forces acting on the body. The electric field effect increases by increasing imposed voltage and decreases by increasing Re number.

**Keywords:** Air Flow, Drag, Electrohydrodynamics, Lift, Numerical Solution

**Reference:** Ashna, M., "Numerical Investigation to Electrohydrodynamic Effect on Lift and Drag Forces on an Airfoil in Low Reynolds Air Flow", *Int. J of Advanced Design and Manufacturing Technology*, Vol. 7/ No. 4, 2014, pp. 77-85.

**Biographical notes:** M. Ashna received his MSc in Mechanical Engineering from University of Tabriz in 2005. He is a lecturer in Islamic Azad University, sanandaj branch and currently a PhD student at Department of Mechanical Engineering, University of Tehran. His research interest includes Numerical Simulation, Electrohydrodynamics, Combustion, Microfluidics and Renewable Energies.

## 1 INTRODUCTION

Applying a high voltage electric field between a thin wire and a conductor plate affects the dielectric fluid by ion injection from the wire. These ions move toward the plate electrode inducing an electronic or ionic flow, which is called corona wind. This corona wind collides with the neutral fluid particles and changes their momentum. It creates a secondary flow crosswise with respect to the main flow and affects heat and momentum transfer [1]. The electrohydrodynamic (EHD) actuator using corona wind is an active method for molecule momentum change. It has several advantages: It is noiseless; it has low power consumption and is easily controllable and applicable to complex geometries. The corona wind effect will be augmented by increasing the applied voltage, where the electrical breakdown strength of fluid must be known and should not be exceeded. Poor design may result in electrical breakdown, which makes the EHD actuator system useless [1], [2].

Seyed-Yagoobi and Owsenak investigated the theoretical and experimental works on EHD heat transfer enhancement through wire-plate corona discharge in air flow over a horizontal surface with constant heat flux [1]. Allen and Karayanis and Seyed-Yagoobi and Bryan published review papers for enhancement of heat transfer and mass transport in single phase and two phase flows with EHD [3], [4]. They showed the importance of this method in extensive applications. Ahmedou and Havet carried out a numerical study on the electrohydrodynamic enhancement of the heat transfer in a channel flow [5]. In the channel flow, the ionic wind was produced by multiple coronating wires. They analyzed the effects of some process parameters (distance between electrodes, wire radius, applied voltage) on the flow and the convective heat transfer enhancement. The model revealed that similar flows could be achieved with different combinations between the inter-electrode distance and the applied voltage.

Kasayapanand investigated the effect of electric field on the natural convection in the square enclosures with single and multiple fins with numerical simulation [6]. The parameters considered were the supplied voltage, Rayleigh number, size of enclosure, electrode arrangement, number of fins, and fin length. The heat transfer enhancement was a decreasing function of Rayleigh number. Moreover, the heat transfer coefficient was substantially improved by the electric field effect especially at high numbers of fins and long fin length.

Nasiri Vatan and others studied experimentally the effect of the corona wind on the natural convection at a rectangular channel [7]. The results indicate that the natural convection in the absence of corona wind at

obtuse angles outperforms than acute angles and keeps improving by increasing the angle. However, the efficiency of the corona wind at acute angles is higher than obtuse angles. Generally, in the presence of corona wind, heat transfer coefficient is increased, while the effect of the corona wind is decreased by raising heat flux. Compared to the large volume of literature dealing with the corona discharge and EHD flow for heat transfer enhancement or pumping, publications related to the altering transaction forces are rare.

Sosa and Artana studied the effects produced by an EHD actuator on the flow around an airfoil at low Re numbers [8]. The analysis was undertaken from flow visualizations and measurements of the surface pressure distributions. The experiments indicate that for low Re number, the effects of the actuation depends on the power added to the flow and on the relative distance between the actuator and the separation line.

Brown and Lai evaluated the characteristics of EHD gas pumps experimentally [9]. They used two tubes of different sizes to house the EHD gas pumps. Experiments were conducted using positive direct current with voltage varying from 13 kV to 30 kV. The results showed that the ionic wind velocity increases to a maximum value and then decreases to an asymptotic value. Kim et al., reported the experimental and theoretical analysis of the ionic wind velocity and electrical-to-kinetic energy conversion efficiency in a corona wind generator with six stages in series [10]. Each stage contained a pair of cylindrical multipin-to-ring electrodes. The experiments were carried out in a negative DC corona discharge and results showed that both the velocity and efficiency are proportional to the square root of the stages number.

Yu Zhang et al., investigated the DC corona discharge in air flow and the induced ionic wind in the needle-to-water system at atmospheric pressure [11]. The water deformation was measured under various conditions. The effects of applied voltage, gap spacing and tip radius on the corona ionic wind were studied. The results indicate that higher voltage or electric field strength results in a stronger ionic wind, while the active area increases with applied voltage below a voltage threshold.

In this paper, a finite volume numerical method is used for simulating electric field and electric current created by a wire-plate EHD actuator. These wires and plate electrodes are placed in specific locations on an airfoil; and the effect of changing positive and negative electrodes, imposed voltage and Re number on drag and lift coefficients are investigated. In section 2, equations describing the phenomena are introduced. In section 3, boundary conditions and numerical procedure used for linking electric field and fluid flow equations, are described. In sections 4 and 5, validation and results are presented.

**2 THEORETICAL APPROACH**

**2.1 Governing Equations**

In order to analyze interaction between an electric field and fluid flow, distribution of electric field must be determined. The electric field is generally calculated through Gauss's law and conservation of electric current relation, where the Gauss's law is defined as follows [4].

$$\vec{\nabla} \cdot \vec{D} = \rho_e \tag{1}$$

The free electric charges produced by electric field in a dielectric fluid, are mostly of the same sign. Therefore, the electric displacement vector is:

$$\vec{D} = \epsilon_e \vec{E} + \vec{P}_e \tag{2}$$

The electric field vector  $\vec{E}$  and polarization vector  $\vec{P}$  are defined as:

$$\vec{E} = -\vec{\nabla} V_e \tag{3}$$

$$\vec{P}_e = \epsilon_e (\kappa - 1) \vec{E} \tag{4}$$

In this study it is assumed that the polarization vector is zero because it is very small for imposed voltage ranges in the air flow. By substitution of  $\vec{D}$  and  $\vec{E}$  from equations (3) and (4) in equation (1) the final form of Gauss's law becomes:

$$\nabla^2 V_e = -\frac{\rho_e}{\epsilon_e} \tag{5}$$

Electric charge density can be determined from conservation of electric charges.

$$\vec{\nabla} \cdot \vec{J} + \frac{\partial \rho_e}{\partial t} = 0 \tag{6}$$

Many EHD phenomena can be successfully modeled by ohmic conduction [4]. Thus the current density  $\vec{J}$  mentioned in equation (6) is defined as:

$$\vec{J} = \sigma \cdot \vec{E} + \rho_e \cdot \vec{U} + \rho_e \cdot \beta \vec{E} \tag{7}$$

The terms on the right hand side represent the conduction, convection and ionic mobility respectively. In a dielectric fluid as air when the current is produced by injection, the first and second terms are negligible [4]. By substitution of  $\vec{J}$  in equation (6) the final case of conservation of electric current becomes:

$$\epsilon_e \cdot \vec{E} \cdot \nabla \rho_e = -\rho_e^2 \tag{8}$$

The electric body force density acting on the fluid becomes [12]:

$$\vec{f}_e = \rho_e \vec{E} \tag{9}$$

This body force will be added as a source term in the momentum equation. The incompressible fluid flow equations without heat transfer consist of:

- Continuity for steady state flow:

$$\vec{\nabla} \cdot \vec{U} = 0 \tag{10}$$

- Conservation of momentum for steady state flow:

$$\vec{U} \cdot \vec{\nabla} \vec{U} = -\frac{1}{\rho} \vec{\nabla} P + \nu \nabla^2 \vec{U} + \frac{1}{\rho} \rho_e \vec{E} \tag{11}$$

The uncoupled equations (5), (8), (10) and (11) should be discretized for iterative solution.

**3 NUMERICAL PROCEDURE AND BOUNDARY CONDITION**

**3.1. Geometry and Boundary Conditions**

Fig. 1 shows the schematic geometry of the solution domain. In this figure, D is the chord line of the airfoil. The dimensions of inlet and outlet lengths are large enough to avoid interference of boundary condition on solution. The airfoil profile is NACA2412 and the attack angle is set to zero. Fig. 2 shows the location of the electrodes on the airfoil.

Both electrodes are on the surface of airfoil and the angle between them regarding the center of front curve of airfoil is 45° for maximum EHD effect [13]. Two possible cases had been studied. In the first case, electrode No. 1 is a wire of 1mm diameter with negative voltage (injector), and electrode No. 2 is a plate of 4mm width with zero voltage (Collector). In the second case, the location of electrodes are changed.

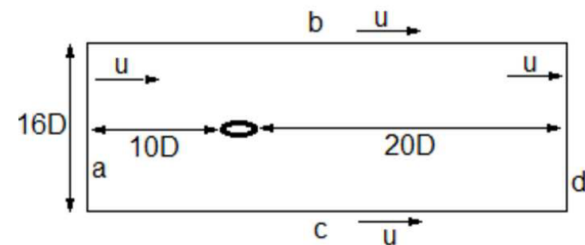


Fig. 1 Schematic geometry of the solution domain

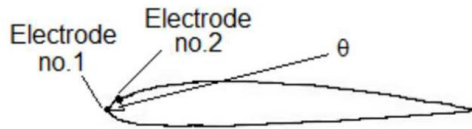


Fig. 2 Location of electrodes on airfoil

For the geometry shown in Fig. 1 the following electric boundary conditions are used:

Along a, b, c, d and airfoil surface (not electrodes):

$$\frac{\partial \rho_e}{\partial \vec{n}} = 0, \frac{\partial \vec{E}}{\partial \vec{n}} = 0 \tag{19}$$

Where  $n$  is an arbitrary unit vector. Along injector electrode:

$$V_e = V_{e0} \text{ and } \rho_e = \rho_{e0} \tag{20}$$

A method of trial and error iteration is used for charge density of injecting electrode surface. First, a primitive value for  $\rho_e$  is guessed, then the electric current from injection electrode to collector electrode is calculated. This current is compared with information available in technical literature. The most important parameters affecting current between electrodes are the electrode shape, distance between electrodes, and the imposed voltage. From the assumption used by a large number of authors [3], [4], [14], [15], and for prevention of breakdown phenomenon in dielectric media, it is recommended to limit the electric current around  $\mu\text{A}$  to few mA. The imposed voltage and electric current quantities used in numerical solution are shown in Table 1.

Table 1 Electrode current due to imposed voltage

Imposed voltage (kV)	Current ( $\mu\text{A}$ )
5	70
10	110
15	160
20	220

Along collector electrode:

$$V_e = 0 \tag{22}$$

For the flow of air in domain we have:

Along a, b, and c:

$$u = U_0, v = 0 \tag{23}$$

And along d:

$$\frac{\partial u}{\partial x} = 0 \tag{24}$$

### 3.2. Numerical Procedure

Steady state electric field equations with steady state and incompressible fluid flow equations are solved numerically. Fig. 3 presents the procedure of solving equations.

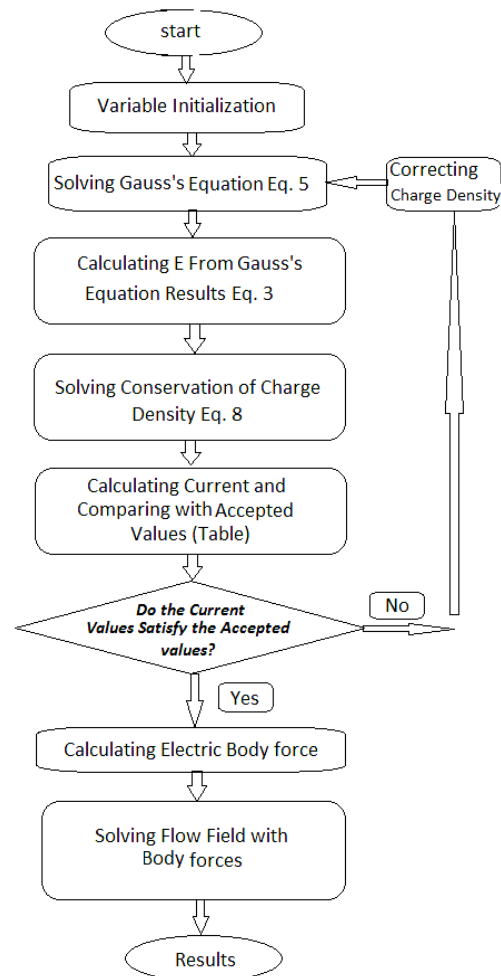


Fig. 3 Flow chart presenting the procedure of solving equations

The electric equations (Eq. 5 and Eq. 8) are not coupled with fluid flow equations, therefore first, electric equations are solved until they converge to an accepted current due to table 1. The results are used to calculate the electric body force. This body forces are set as source term in Navier-Stokes equations. The continuity

equation is solved to correct the variable values and this procedure is pursued until it converges. Equations are discretized in the standard form of the finite volume method using the upwind scheme. The SIMPLE algorithm is applied for numerical procedure assuming the material properties to be constant. The mesh is refined to gain independence of mesh solution where a final and unique size is used for all cases.

## 4 RESULTS AND DISCUSSION

### 4.1. Validation

To validate the code, a similiar experimental work was simulated. Sosa and Artana have studied the effect of EHD actuator on laminar boundary layer behaviour on a NACA 0015 airfoil [8].

Fig. 4 presents a comparison of Sosa’s experimental pressure coefficient distribution on the upper surface, in zero attack angle and air velocity of 3.6 m/s with numerical results by our code. Fig. 5 shows this comparison for the lower surface of the wing. Although curves don’t adapt exactly, however they demonstrate good agreement in pattern.

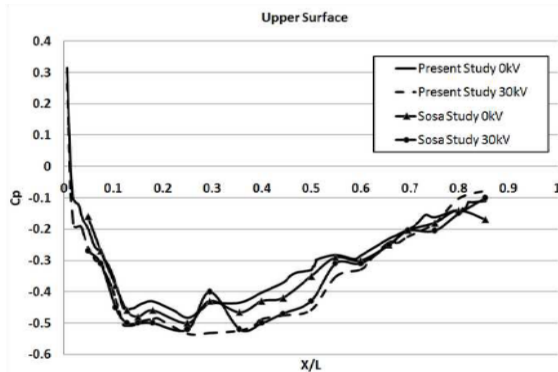


Fig. 4 A comparison of Cp distribution on upper surface of the NACA 0015 airfoil reported by Sosa and present study

### 4.2. Results

Fig. 6 shows electrical potential distribution around the profile when electrode No.1 is active electrode. The electrical potential is directly proportional with imposed voltage. Fig. 7 shows the electrical field intensity calculated from electrical potential by equation (3). The electric field intensity is very high around sharp wire electrode and is moderate around plate electrode. It’s due to rapid change in electrical potential around sharp electrode. Far away from electrodes where the potential is constant or changes smoothly, the electrical field intensity reaches its minimum values.

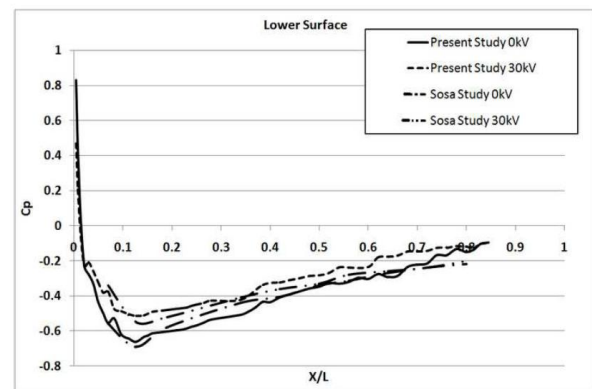


Fig. 5 A comparison of Cp distribution on lower surface of the NACA 0015 airfoil reported by Sosa and present study

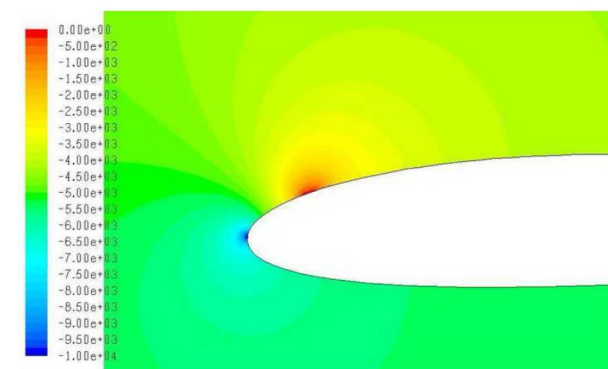


Fig. 6 Electric potential distribution around electrodes when electrode No.1 is the active electrode

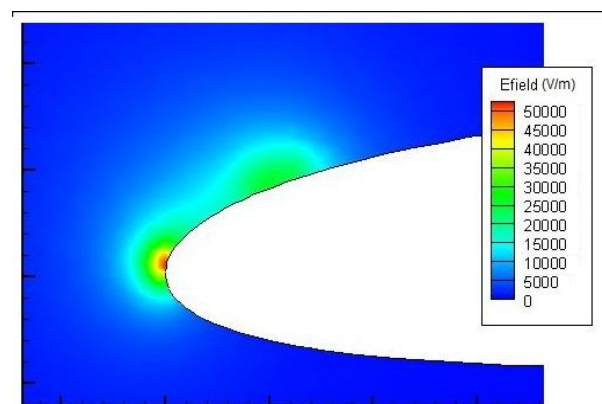
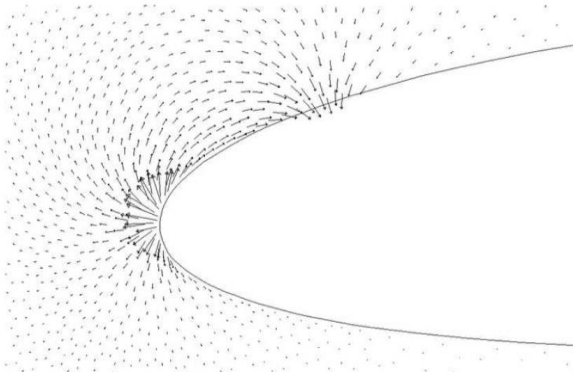


Fig. 7 Electric field distribution around electrodes when electrode No.1 is the active electrode

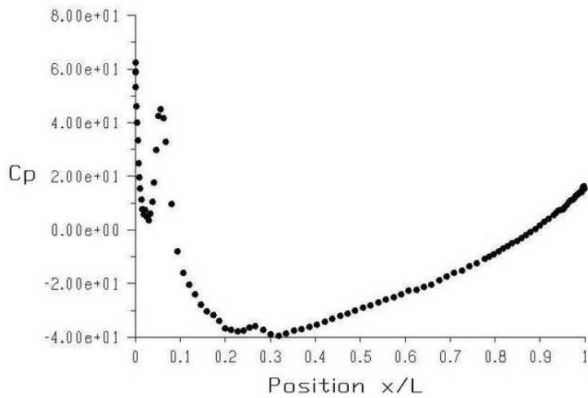
Fig. 8 represents the body force vectors when electrode No.1 is the active electrode. The electric current is from electrode No.1 to electrode No. 2, therefore a weak field of body force vectors is produced from electrode No. 1 to electrode No. 2. However the vectors are noticeably magnified to be clearly observed; the force

pattern shows that it inclines the flow towards the surface. These body forces change the momentum of main flow, thus affecting the pressure coefficient.



**Fig. 8** The body force vectors when electrode No.1 is the active electrode

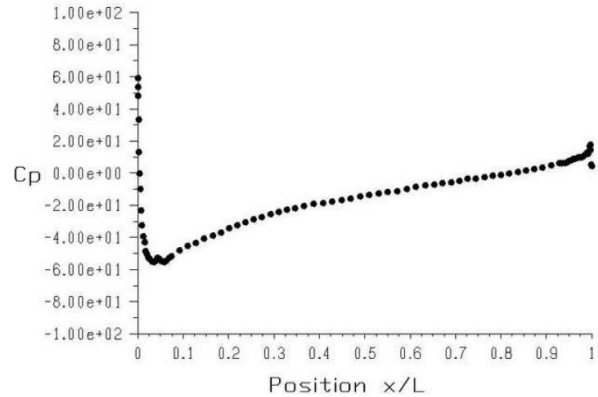
Fig. 9 shows the pressure coefficient through the upper surface of the airfoil when a 10kV negative voltage is imposed on electrode No.1 and free air flow has 10m/s velocity. It is apparent that  $C_p$  curve has a local augment around the electrode and a general augment through the curve. These augments are produced by changes in air flow pattern created by eclectic body forces near electrode.



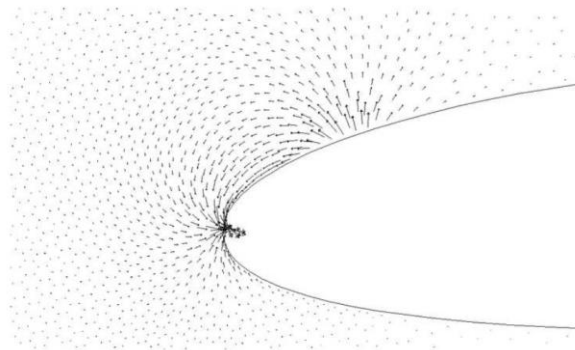
**Fig. 9** Pressure coefficient through the upper surface of the airfoil when a 10kV negative voltage is imposed on electrode No.1 and free airflow of 10m/s velocity.

Fig. 10 illustrates that changes in pressure coefficient beneath the airfoil are not as much as above the airfoil, because no electric current flows there. Fig. 11 represents the body force vectors when electrode No. 2 is the active electrode. The electric current is from electrode No. 2 to electrode No. 1, therefore a weak field of body force vectors is produced from electrode No. 2 to electrode No. 1. However the vectors are

noticeably magnified to being clearly observed, hence the force pattern shows that it is against the fluid flow.



**Fig. 10** Pressure coefficient through the beneath surface of the airfoil when a 10kV negative voltage is imposed on electrode No. 1 and free air flow of 10m/s velocity.



**Fig. 11** The body force vectors when electrode No. 2 is the active electrode.

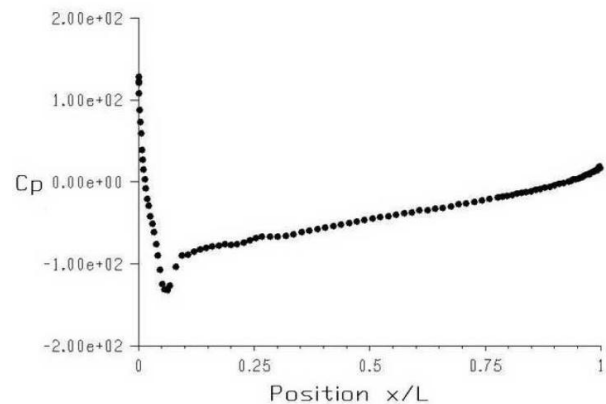


**Fig. 12** Pressure coefficient through the upper surface of the airfoil when a 10kV negative voltage is imposed on electrode No. 2 and free air flow has 10m/s velocity

Fig. 12 shows the pressure coefficient through the upper surface of the airfoil when a 10kV negative voltage is imposed on electrode No. 2 and free air flow has 10m/s velocity.  $C_p$  curve has a local decrease around the electrode and a general decrease through the curve. These decreases are produced by changes in air flow pattern created by eclectic body forces near the electrode.

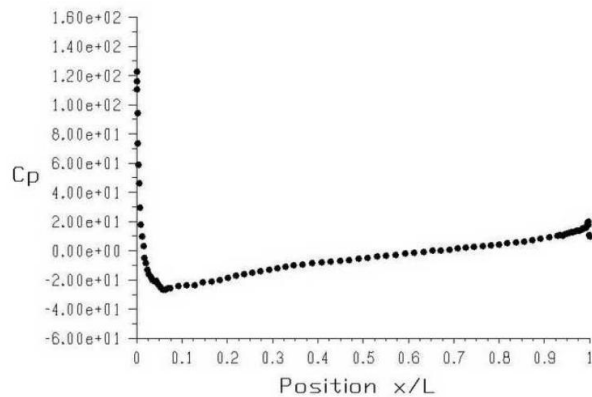


Fig. 13 Pressure coefficient through the beneath surface of the airfoil when a 10kV negative voltage is imposed on electrode No. 2 and free air flow has 10m/s velocity

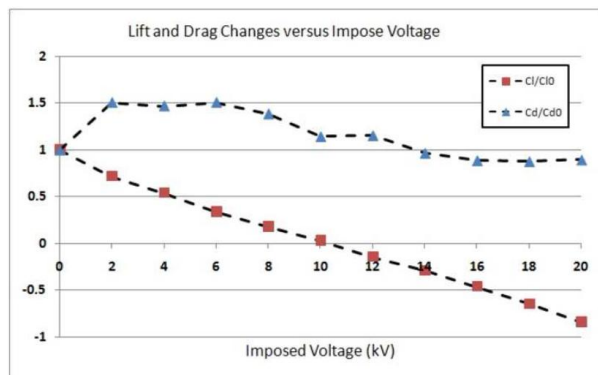


Fig. 14 Imposed voltage effect on lift and drag coefficients when electrode No. 1 is active and the air velocity is 10m/s.

Fig. 13 illustrates that changes in pressure coefficient beneath the airfoil are not as much as above the airfoil. It's because no electric current flows there. Fig. 14 shows the imposed voltage effect on proportional lift and drag coefficients when electrode No. 1 is active and the air velocity is 10m/s. The proportional drag and lift coefficients are defined as ratio of this coefficient with imposed voltage to without imposed voltage. The curves characterize that the proportional drag coefficient increases first with imposed voltage and then declines to a constant value. Proportional lift coefficient decreases at a constant rate with imposed voltage. Fig. 15 shows the imposed voltage effect on

proportional lift and drag coefficients when electrode No. 2 is active and the air velocity is 10m/s. Proportional drag coefficient decreases slickly with imposed voltage and then declines to a constant value. Proportional lift coefficient increases with a constant rate with imposed voltage.

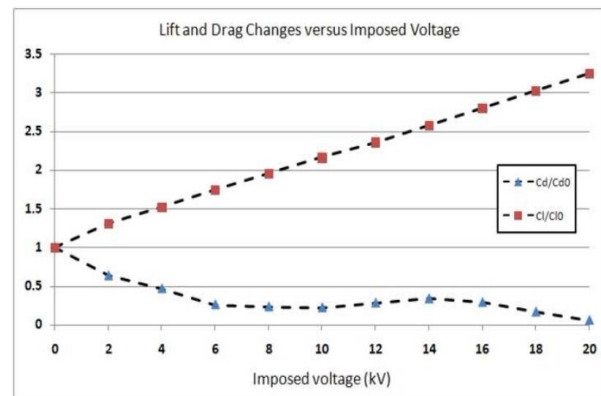


Fig. 15 Imposed voltage effect on proportional lift and drag coefficients when electrode No. 2 is active and the air velocity is 10m/s.

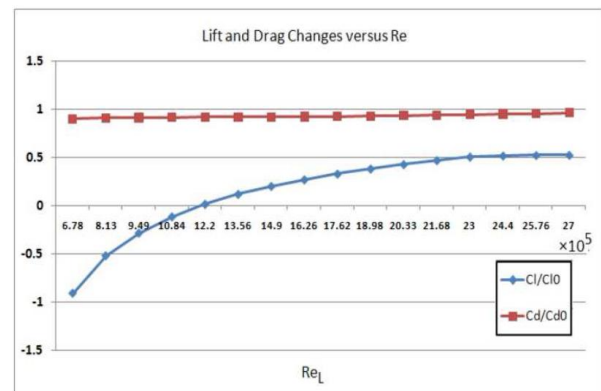
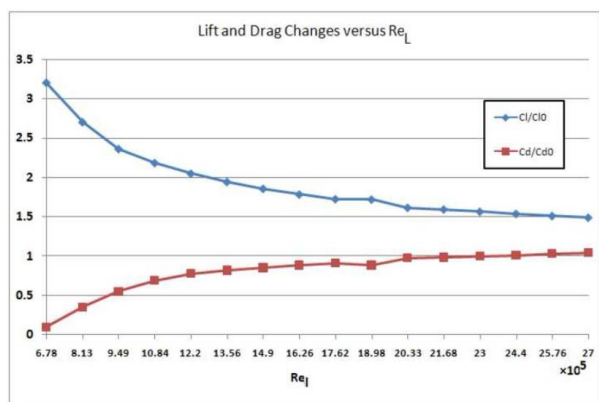


Fig. 16 Reynolds effect on lift and drag proportional coefficients when electrode No. 1 is active and the imposed voltage is 20kV.

Fig. 16 shows the Reynolds number effect on proportional lift and drag coefficients when a 20kV voltage is imposed on electrode No. 1. It's obvious that both proportional lift and drag coefficient decreases due to  $Re_L$ .

It's because the momentum of fluid increases due to Re number and the body force affecting it weakens. Fig. 17 shows the Reynolds number effect on proportional lift and drag coefficients when a 20kV voltage is imposed on electrode No. 2. In this case proportional lift coefficient decreases to a constant ratio but drag coefficient increases due to  $Re_L$ .



**Fig. 17** Reynolds effect on lift and drag proportional coefficients when electrode No. 2 is active and the imposed voltage is 20kV.

## 5 CONCLUSION

A numerical study of controlling flow on an airfoil with zero attack angle was performed using a corona actuator, where the results can be summarized as follows:

1. The actuator can change local pressure coefficient severely on the surface where the electrodes are placed. The effect of actuator on other surface pressure coefficient is insignificant.
2. The set up of electrodes is very important. When electrode No. 1 is a negative injector, it reduces lift coefficient and has a weak effect on drag coefficient. While when electrode No. 2 is a negative injector it increases lift coefficient and decreases drag coefficient significantly.
3. Increasing imposed voltage increases the effect of actuator in both set ups.
4. Increasing Re number decreases the effect of actuator. It is because in high Re flow, the momentum of fluid particles is so much that the corona wind cannot change their momentum significantly.
5. Although the study was performed for a wide range of Re numbers, it is seen that the actuators effect is considerable for  $Re < 100000$ .
6. The results show that for local and mean values of pressure coefficient changes in low Reynolds numbers a system of wire-plate electrodes is suitable. For higher Reynolds numbers a single wire-plate system is not effective.
7. EHD actuator may be a good idea for controlling lift and drag forces in light airplanes such as light drones, it may also be used for prevention of separation.

## 8 NOMENCLATURE

$D$	[FV/m <sup>2</sup> ]	Electric Displacement vector
$E$	[V/m]	Electric field intensity vector
$EO$	[V/m]	Electric field intensity on wire
$fe$	[N/m <sup>3</sup> ]	Electric body force
$I$	[A]	Electric current
$J$	[A/m <sup>2</sup> ]	Electric current vector
$LoE$	[-]	Lorentz force number
$n$	[-]	local unit normal vector
$NE$	[-]	electric field number
$P$	[Pa]	Pressure
$Pe$	[FV/m <sup>2</sup> ]	Polarization vector
$Pr$	[-]	Prandtl number
$Re$	[-]	Reynolds number
$t$	[s]	Time
$u$	[m/s]	Velocity vector
$U$	[m/s]	Velocity vector
$Ve$	[V]	Electric potential
$B$	[m <sup>2</sup> /V.s]	Mobility of the ions in gas
$Ee$	[F/m]	Permittivity of the medium
$K$	[-]	Dielectric constant
$\nu$	[m <sup>2</sup> /s]	Fluid kinematic viscosity
$\sigma$	[S/m]	Electric conductivity
$\rho$	[Kg/m <sup>3</sup> ]	Density
$\rho e$	[C/m <sup>3</sup> ]	Charge density

### Subscripts

- 0 On the wire (electrical parameters)

## REFERENCES

- [1] Seyed-Yagoobi, J., Owsenesk, B. L., "Theoretical and experimental study of electrohydrodynamic heat transfer enhancement through wire-plate corona discharge", Journal of Heat Transfer, Vol. 119, 1997, pp. 604-610.
- [2] Mohseni, H., "Advanced electrical high voltage engineering", 5th ed., Tehran University Press, 1998, Chap 3.
- [3] Allen, P. H. G., Karayanis, T. G., "Electrohydrodynamic enhancement of heat transfer and fluid flow", Heat Recovery Systems, Vol. 15, No. 5, 1995, pp. 389-423.
- [4] Seyed-Yagoobi, J., Bryan, J. E., "Enhancement of heat transfer and mass transport in single-phase and two-phase flows with EHD", Advances in Heat Transfer, Vol. 33, 1999, pp. 95-104.
- [5] Ahmedou, O. A., Havet, M., "Effect of process parameters on the EHD airflow", Journal of Electrostatics, Vol. 67, 2009, pp. 222- 227.
- [6] Kasayapanand, N., "A computational fluid dynamics modeling of natural convection in finned enclosure under electric field", Applied Thermal Engineering, Vol. 29, 2009, pp. 131-141.
- [7] Nasiri Vatan, S., Merdasi, A., "Empirical correlation for performance evaluation of electric/corona wind on

- natural convection”, *Journal of Electrostatics*, Vol. 72, No. 1, 2014, pp. 82-90.
- [8] Sosa, R., Artana, G., “Steady control of laminar separation over airfoils with plasma sheet actuators”, *Journal of Electrostatics*, Vol. 64, 2006, pp. 604-610.
- [9] Brown, N. M., Lai, F. C., “Electrohydrodynamic gas pump in a vertical tube”, *Journal of Electrostatics*, Vol. 67, 2009, pp. 709-714.
- [10] Kim, C., Park, D., Noh, K. C., and Hwang, J., “Velocity and energy conversion efficiency characteristics of ionic wind generator in a multistage configuration”, *Journal of Electrostatics*, Vol. 68, No. 1, 2010, pp. 36-41.
- [11] Zhang, Y., Liu, L., and Ouyang, J., “On the negative corona and ionic wind over water electrode surface”, *Journal of Electrostatics*, Vol. 72, No. 1, 2014, pp. 76-81.
- [12] Melcher, J. R. *Continuum Electromechanics*, MIT Press, 1981.
- [13] Ashna, M., Azizadeh, B., and Goodarzi, M., “Numerical investigation of electrode position on EHD effect on forces imposed on a cylinder in air flow”, *ISME2011 Proceeding*, 2011.
- [14] Takimoto, A., “Convective heat transfer enhancement by a corona discharge”, *Transactions of JSME*, Vol. 54, 1988, pp. 695-703.
- [15] Darabi, J., Rhodes, C., “CFD modeling of an ion-drag micropump”, *Journal of Sensors and Actuators*, Vol. 127, 2006, pp. 94-103.